Biologically Induced Reduction in Symmetry: A Study of Crystal Texture of Calcitic Sponge Spicules

Joanna Aizenberg, Jonathan Hanson, Thomas F. Koetzle, Leslie Leiserowitz, Stephen Weiner, and Lia Addadi*

Abstract: Organisms can exert a remarkable degree of control over crystal growth. One way of achieving this is by the adsorption of specialized macromolecules on specific planes of the growing crystals. With continued growth of the crystal, the macromolecules are incorporated inside the crystal bulk. Their presence does not change the crystal structure, but creates discontinuities in the perfect lattice. Here we study in detail three unusual cases of reduction in symmetry at the level of crystal domain shapes, induced by this controlled intercalation. We examined sponge spicules, which are single crystals of Mg-bearing calcite. They were specifically chosen for this study, because their morphologies do not reflect the hexagonal symmetry of calcite. Their crystal textures (coherence lengths and angular spreads) were characterized by high-resolution X-ray diffraction with well-collimated synchrotron radiation. The results are compared to analogous studies of synthetic calcite and Mg-bearing calcite. In all the selected spicules reduction in symmetry is observed in the coherence lengths among symmetry-related crystallographic directions. The reconstructed shapes of the domains of perfect structure closely match the specific spicule morphologies. The synthetic crystals show no such reduction in symmetry. Although the manner by which such exquisite control is achieved is not known, we envisage it involving a combination of oriented nucleation with either physical or stereochemically driven adsorption.

Keywords
biomineralization · calcite · crystal morphology · mosaic structure · symmetry reduction

Introduction

In the course of evolution, nature has developed strategies that endow biological processes with exquisite specificity and selectivity. The implications of this almost trivial statement are wonderfully exemplified in the realm of crystal formation by organisms.

Crystals are used by organisms for a wide variety of purposes, the most common of which is to provide stiffness to their skeletal parts. Even some of the most primitive species exercise a level of control over crystal nucleation, growth and material properties that is almost unthinkable in artificial crystallization processes.[1] In particular, organisms do appear to recognize and exploit symmetry and intrinsic structural characteristics of crystals when beneficial, but are able to "overcome them at will" when necessary. Control over crystal formation is achieved in a variety of ways at the cellular level and at the molecular level by means of specialized macromolecules. Some of the latter are adsorbed on specific faces of the growing crystals, and with continuing growth are incorporated inside the crystal bulk.[2] This and other strategies used to control single crystal texture and morphology result in an effective reduction in crystal symmetry at the level of the microscopic domain shape. They are the focus of this study.

Reduction in morphological symmetry has been observed in various biologically formed single crystals.[1c] Reduction in crystal lattice symmetry has been described in a number of different molecular[3] and inorganic[4] systems. This was achieved by selective substitution of an additive in a subset of sites that are nominally symmetry-related in the unit cell. The basic concept underlying this phenomenon is quite simple: addition of foreign molecules to a growing crystal always occurs at surfaces, whose symmetry may be lower than in the bulk structure. The incorporation of foreign molecules is thus dictated by the orientation and availability of each specific site at the particular surface. The bulk structure in each growth sector reflects the reduced symmetry of the face through which addition occurred. Furthermore, in a crystal formed of prochiral molecules, symmetry may be reduced by site-selective introduction of a chiral additive at enantiotopic sites.[5]

The additive molecules in all the cases described to date are sufficiently similar to the basic component of the crystal to enable incorporation in the lattice as a solid solution. Macromolecules, such as the proteins and glycoproteins present within biogenic crystals, are orders of magnitude larger than the unit cell of a small molecule or inorganic salt, and are not expected

[*] Prof. L. Addadi, J. Aizenberg, Prof. S. Weiner
Dept. of Structural Biology, Weizmann Institute of Science
Prof. L. Leiserowitz
Dept. of Materials and Interfaces, Weizmann Institute of Science
Rehovot (Israel)
Telefax: Int. code + (8)344-136
e-mail: csaddadi@weizmann.weizmann.ac.il
Dr. J. Hanson, Dr. T. F. Koetzle
Chemistry Dept., Brookhaven National Laboratory
Upton, NY (USA)

0947-6539/95/0107-0414 $ 30.00+.25/0

to be incorporated inside the perfect crystal lattice. We have demonstrated that such macromolecules are preferentially located on specific crystal planes.[6] We inferred that they are located at the boundaries of domains of perfect structure, creating or stabilizing such imperfections and subsequently influencing the crystal texture, rather than its bulk structure.[7] These effects were monitored through measurements of X-ray diffraction peak broadening performed at high resolution with synchrotron radiation in the $\omega/2\theta$ mode, to yield the crystal coherence lengths, and in the ω mode, to yield the alignment parameters of the crystals. The specimens examined included a series of biogenic calcite single crystals from sea urchin spines, teeth and larval spicules, mollusk and foraminifer shells, and calcareous sponge spicules, as well as some artificial model systems.[7] We showed that the coherence lengths (or sizes of perfect domains) are well correlated with the anisotropic intercalation of proteins in specific directions that are related to the growth mode of the crystal. It was also shown that when no macromolecules are present within the calcite crystals examined, an isotropic texture is present, such as that of synthetic calcite.[8] We suggested that this intercalation is part of a complex concerted strategy used for the control of morphology, as well as material properties of the biogenic crystals.[8] Here we shall describe analogous synchrotron X-ray diffraction measurements on three types of sponge spicules, highlighting the aspect of reduction in symmetry.

The sponges (*Porifera*) are among the most primitive of animal phyla. Many members of this phylum form spicules composed of amorphous silica. One group (*Calcarea*), however, forms spicules composed of the most stable polymorph of calcium carbonate, calcite.[9] Calcite crystallizes in the trigonal centrosymmetric space group $R\bar{3}c$. The crystals of pure calcite develop in a typical "cleavage rhombohedron" morphology, expressing the six {104} faces[10] (Fig. 1 A). Magnesium-containing synthetic calcite crystals develop, in addition, a set of rough {011} faces (Fig. 1 B).[6] In contrast, the spicules of calcisponges adopt a wide variety of morphologies that are often taxonomically specific. Each spicule is a single crystal of magnesium-containing calcite, and the orientations of their crystallographic axes bear a fixed relationship to the spicule morphology (Fig. 1 C–F). One of the most interesting and unusual properties of the spicules chosen for this study is that their macroscopic morphologies do not even reflect the hexagonal symmetry of calcite. The *Kebira* giant monaxon can reach several millimeters in length.[9d] It is elongated in the [012] direction and curved with the convexity always in the positive direction of the *c* axis (Fig. 1 D). The *Kebira* "nail" spicule is a nail-shaped cylindrical element (about 300 μm long),[9d] with its main morphological axis elongated in a direction oblique to the crystallographic axis *c* by roughly 35°, between $[0\bar{1}5]$ and $[0\bar{1}6]$ (Fig. 1 E). The *Sycon* giant triact[9b] has two rays elongated in symmetry-related directions, $[\bar{1}02]$ and $[1\bar{1}2]$, but the third is elongated along $[0\bar{1}6]$ (Fig. 1 F). They occasionally have a fourth ray, which develops in a direction that is symmetry-related to the third.

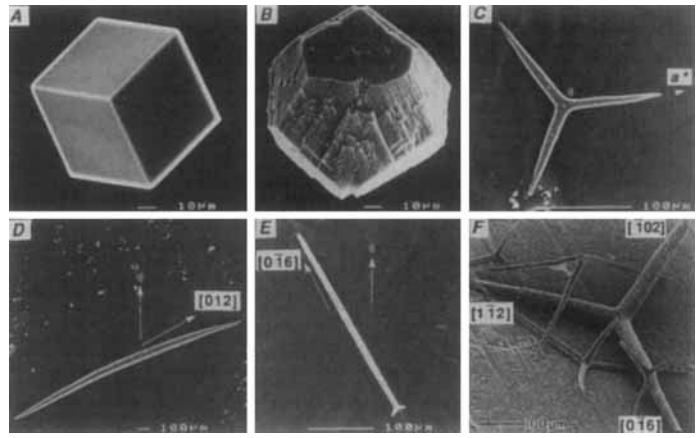

Fig. 1. Scanning electron micrographs of the calcite crystals studied. A) Pure synthetic calcite. B) Synthetic Mg-bearing calcite. C) Symmetric triradiate spicule from the calcareous sponge *Clathrina contorta*. D) Curved monaxon spicule from *Kebira uteoides*. E) "Nail" spicule from *Kebira* sp. F) Asymmetric triradiate spicule from *Sycon* sp. The orientations of the crystallographic axes relative to the spicule morphology are indicated.

It will be shown that all these spicules display reduced symmetry at the textural level. The reduction in symmetry is in every case correlated to the crystal morphology and, through this, to the mechanism of crystal growth. The possible mechanistic explanations of this phenomenon will also be discussed.

Results

The diffraction peak profiles in the ω and $\omega/2\theta$ scan modes were monitored for one pure synthetic calcite crystal, two synthetic Mg-calcite crystals, three giant curved *Kebira* monaxons, one naillike *Kebira* spicule, and four *Sycon* asymmetric triradiate spicules. For greater reliability of interpretation, two spicules of the latter type were measured intact, two others were subdivided into three different rays, and each was studied separately. For comparison to the other spicules, we also show the data for one of the *Clathrina* triradiate spicules that have been reported separately.[8] The following {*hkl*} families of reflections were monitored: {104}, {018}, {012}, {0012}, {006}, {110}, {030}, and {202}, and for several crystals also {024}, {113}, {1010}, $\{\bar{1}\bar{1}6\}$, {116}, and {1112}. Three crystallographically equivalent reflections were measured for each of these families.[10] For Friedel pairs, the results were assumed to be equal. Thus, crystal imperfections in different crystallographic directions, as well as within a set of symmetry-related directions, could be examined. Representative diffraction peak profiles obtained for one crystal of each type are shown in Figure 2. The diffraction vectors of

Editorial Board Member:[*] *Lia Addadi was born in Padua (Italy) in 1950, studied organic chemistry at the Università degli Studi di Padova from 1968 to 1973. She then transferred to the Weizmann Institute of Science Israel where she completed her Ph.D. in 1979. After her postdoctoral stay with J. R. Knowles at Harvard (1981–1982) she returned to the Weizmann Institute, where she became Associate Professor in 1988 and Full Professor in 1993. Her research interests include biomineralization, pathological crystallizations, protein–crystal interactions, protein adsorption, and cell adhesion to solid substrates.*

[*] Members of the Editorial Board will be introduced to the readers with their first manuscript.

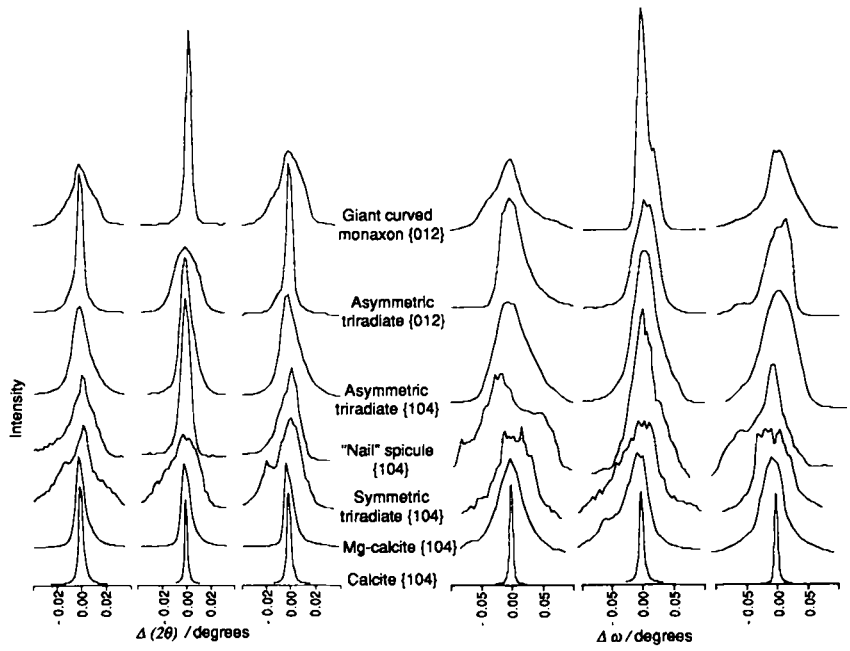

Fig. 2. Representative sets of three symmetry-related diffraction peak profiles {012} or {104} for the different crystals, showing how one of the three symmetry-related reflections differs from the other two in the crystallographically asymmetric biogenic crystals. $\omega/2\theta$ scan mode (left) and ω scan mode (right).

the reflections presented, namely, the {104} and {012} sets,[10] were chosen because they coincide with the morphological axes directions of the different biogenic crystals examined here. Surprisingly, the $\omega/2\theta$ diffraction peak widths measured for the biogenic crystals vary not only between different crystallographic directions, but also within families of identical crystallographic directions (Table 1, Materials and Methods). Each crystal of the same type, however, shows similar deviations from isotropy. Notwithstanding the differences in peak maximum intensities and peak widths, the integrated intensities of the profiles belonging to the same {*hkl*} family agree moderately well (Table 1). Furthermore, the *d* spacings in the same {*hkl*} family do not change; this shows that the anisotropy is not due to asymmetric incorporation of magnesium or protein in the lattice.[11] These facts confirm that the differences observed are indeed due to anisotropy in crystal texture.

Synthetic calcite crystals: *Pure calcite*: The reflections in both modes of measurements are extremely sharp (Fig. 2). The peak widths at half height were close to the resolution limit of the instrument (0.004–0.007 and 0.005–0.010° for the ω and $\omega/2\theta$ scan modes, respectively). The crystal is texturally almost isotropic (Fig. 3A, B). However, it should be noted that, for each family of crystallographically equivalent planes, there is a typical clustering of the coherence length values calculated for each of the {*hkl*} families of reflections (Fig. 3A). This may be due to the empirical character of the Scherrer formula, which fails to properly take into account the 2θ-dependence of the reflection width,[12] and/or to intrinsic differences in the calcite structure. However, the estimated coherence lengths are almost the same for differently oriented crystallographic planes that diffract at similar Bragg angles (note, for example, the (006) and {110} planes with $\theta = 9.3$ and 10.6°, respectively, or (0012) and {030} planes with $\theta = 18.9$ and 18.6°, respectively). In contrast, for the identical (*hkl*) and (*nh*,*nk*,*nl*) planes that diffract at different Bragg angles, the calculated domain sizes differ significantly (note the (006) and (0012) or {012} and {024} pairs in Fig. 3A).

These differences may also be accounted for by the energy dispersion of the beam at the different 2θ angles. The differences in the peak widths within families of the symmetry-related crystallographic directions are rather small ($R = 6.9$ and 4.9% for the ω and $\omega/2\theta$ scan modes, respectively). Thus, the empirical character of the Scherrer formula, which does not yield constant values for different Bragg angles, and the fact that the peak widths measured are close to the instrumental resolution limit are the main factors responsible for the observed deviations ($\approx 25\%$) from the textural isotropy.

Synthetic Mg-calcite crystals: Growth of calcite in the presence of magnesium ions results in modified crystal morphology (Fig. 1B). Besides the normal {104} habit, the crystals are delimited by an additional stepped {011} family of faces.[6] The total magnesium content within the crystals determined by atomic absorption is 5.8 mol%. However, the magnesium content deduced from the reduction of the cell dimensions accounts for only 3.0 mol%. We infer that 3.0 mol% magnesium is within the crystal lattice in the form of a solid solution, while the remainder is concentrated on the boundaries of crystalline domains. Even such a small amount of a foreign ion affects both textural parameters of calcite. The coherence lengths are isotropically reduced by a factor of 2–3 relative to those of the control pure crystal (Fig. 3C). Clustering of the coherence length values, similar to that of the pure calcite crystal, is observed for different {*hkl*} families of reflections. The main effect caused by the presence of Mg^{2+} on the boundaries is an enormous increase (by a factor of 10–15) of the angular spread of the domains (Fig. 3D). However, both textural parameters remain isotropic. The discrepancy factors between symmetry-related reflections are 7.9 and 10.4% for the coherence lengths and angular spreads, respec-

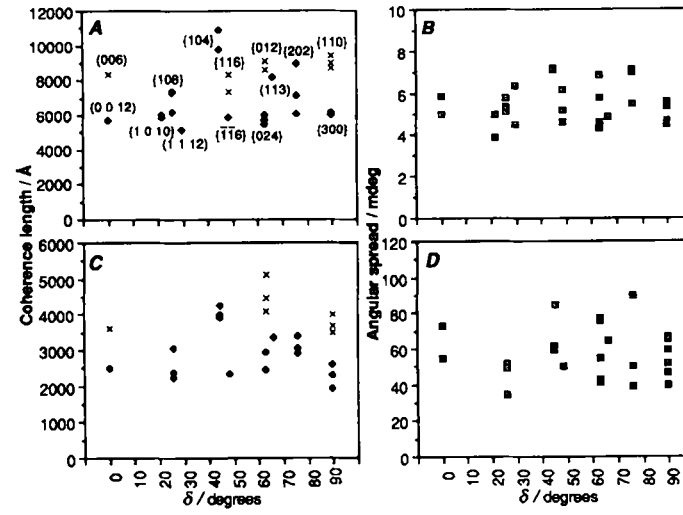

Fig. 3. Coherence lengths (left) and angular spreads (right) for all measured diffraction peak profiles of synthetic calcite crystals, expressed as a function of the dihedral angle (δ) between the diffracting plane and the (001) plane. Different crystallographic families of reflections are indicated. Where two families of crystal planes appear at the same dihedral angle, they are distinguished by different symbols. A–B, pure calcite. C–D, one of the measured Mg-calcite crystals.

0947-6539/95/0107-0416 $ 30.00+.25/0 Chem. Eur. J. 1995, 1, No. 7

tively. This implies that magnesium is homogeneously incorporated within the growing crystals.

Biogenic calcite crystals: The spicules of calcisponges are almost always single crystals of Mg-bearing calcite.[9] However, their surfaces are rounded, smooth, and express none of the stable crystal faces of calcite (Fig. 1C–F). The amounts of magnesium introduced inside the crystal lattice of the calcitic spicules examined here are significantly higher than those obtained in vitro (Table 1). The morphological axes of the spicule rays and the crystallographic axes of the constituent calcite crystal always have a constant spatial relation. This does, however, vary from one species to another and within a species between different spicule types.

In order to facilitate the interpretation of the textural measurements, we eliminate the intrinsic reflection-dependent effect observed in the synthetic calcite crystals. This is achieved by the normalization of each calculated spicule coherence length to the mean coherence length value obtained for the same family of crystallographic planes in the pure calcite crystal.

The morphology of the *Clathrina triradiate spicule* reflects the trigonal symmetry of calcite.[9a] The *c* axis is oriented perpendicular to the plane of the spicule, and the *a** axes are aligned along the rays (Fig. 1C). The average angular spread of the domains is drastically increased compared to the pure calcite crystal, and is roughly the same in all crystallographic directions[8] (Fig. 4B). The average domain sizes are fourfold smaller than those of the control calcite crystal (Fig. 4A). The reduction in coherence length is much greater along the *c* axis than that observed for the coherence length values estimated for the *ab* plane. No anisotropy is observed within families of symmetry-related crystallographic directions. The differences in the diffraction peak widths of the crystallographically equivalent reflections are as small as those observed in the control calcite and Mg-calcite crystals ($R = 7.8$ and 6.7% for the ω and $\omega/2\theta$ scan modes, respectively).

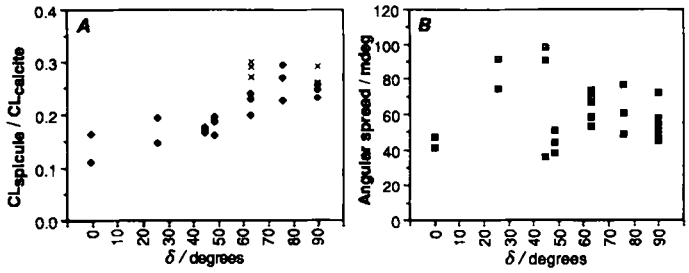

Fig. 4. Coherence lengths normalized to pure calcite (A) and angular spreads (B) for the diffraction peaks of a *Clathrina* triradiate spicule, plotted as a function of the dihedral angle δ (taken from ref. [8]). Where two families of crystal planes appear at the same dihedral angle, they are distinguished by different symbols.

Giant curved monaxons from Kebira[9d] develop in a direction roughly perpendicular to the (012) crystallographic plane and are restricted in growth perpendicular to the symmetry-related ($\bar{1}02$) and ($1\bar{1}2$) planes[10] (Fig. 1D). It is immediately evident that the standard deviations of the coherence length values estimated for the entire data set are unusually high (70–80%). This can be explained by the fact that, in both modes of measurement, the width of one peak in each family of equivalent reflections is systematically different from the other two (Fig. 5A). Significantly, in all cases, the larger coherence lengths are found in the directions coincident with or close to the direction of the spicule morphological axis. In order to visualize this

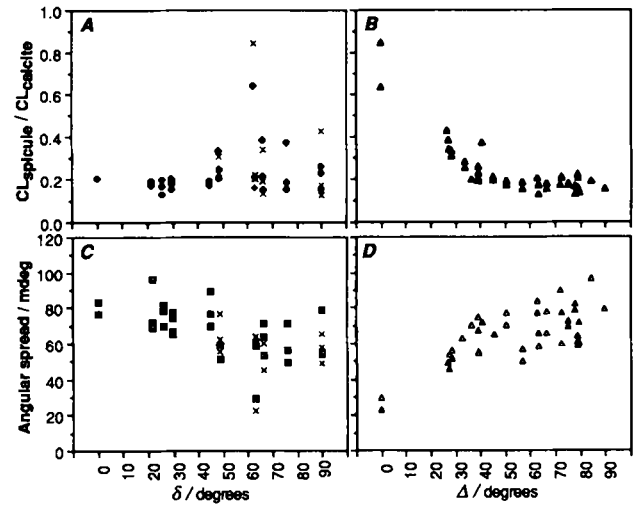

Fig. 5. Textural parameters of one *Kebira* curved monaxon spicule. A) Normalized values of coherence lengths as a function of dihedral angle (δ) between the diffracting plane and the (001) plane. B) Normalized values of coherence lengths, expressed as a function of the angle (Δ) between the diffracting plane and the (012) plane. C) Angular spreads as a function of δ. D) Angular spreads as a function of Δ. Where two families of crystal planes appear at the same dihedral angle, they are distinguished by different symbols.

effect, the coherence lengths are plotted as a function of the angle between the diffracting plane and the (012) plane, which is the plane of symmetry of the spicule (Fig. 5B). In this representation, it is clear that the domain sizes are not randomly distributed, but gradually decrease with increasing deviation of the diffracting vector from the morphological axis direction. In general, the smallest domain sizes (1500 ± 250 Å) are observed in the *ca* plane, which is roughly perpendicular to the longitudinal direction of the spicule. In this plane, the coherence lengths are sixfold smaller than those of the pure calcite crystal and are isotropic, independent of the specific crystallographic orientation within the calcite structure. Domains in the direction perpendicular to the (012) crystallographic plane and roughly parallel to the morphological axis of the spicule, are as large as those in the control calcite crystal (Table 1). The distribution of angular spreads of the domains follows the anisotropic features observed for the coherence lengths (Fig. 5C,D), that is, it is smallest where the coherence length is largest. Thus, in these crystals texture is linked to morphology, but is independent of lattice symmetry. This implies a high degree of biological control over the microenvironment of crystal growth, particularly when taking into account the fact that one direction is differentiated from the other symmetry-related equivalent ones.

"Nail" spicules from Kebira:[9d] The morphological axes of these crystals are oriented at a constant angle of about 35° relative to the *c* crystallographic axis (Fig. 1E). Thus, the spicules grow roughly perpendicular to only one member of the family of the crystallographically equivalent planes {10*l*} ($l \approx 5$–6). The family of reflections closest to this direction that we can monitor is {104}.[10] Anisotropy of both textural parameters is observed within families of symmetry-related reflections for this biogenic element as well (Fig. 6). The coherence length in the direction perpendicular to the ($0\bar{1}4$) plane is 5650 Å, whereas twofold smaller values (2600 and 2750 Å) are found for the directions perpendicular to the symmetry-related ($\bar{1}14$) and (104) planes. The coherence lengths gradually decrease (Fig. 6B) and the angular spreads increase (Fig. 6D), when plotted as a function of the angle between the diffracting plane and the ($0\bar{1}l$) plane.

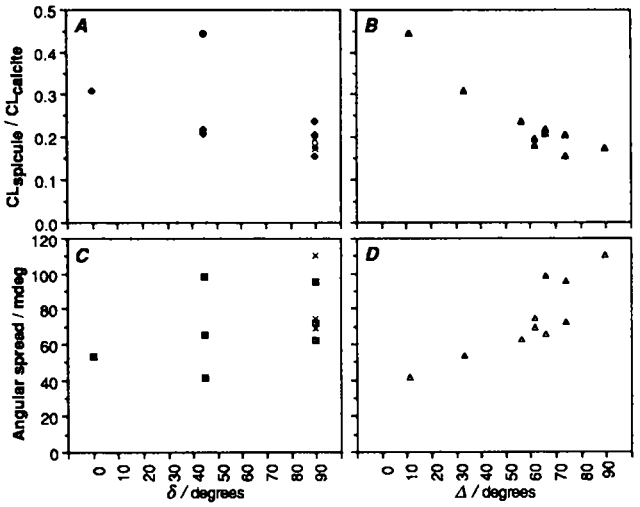

Fig. 6. Textural parameters of *Kebira* "nail" spicule. A) Normalized values of coherence lengths as a function of dihedral angle (δ) between the diffracting plane and the (001) plane. B) Normalized values of coherence lengths, expressed as a function of the angle (Δ) between the diffracting plane and ($0\bar{1}l$) plane ($l \approx 5-6$). C) Angular spreads as a function of δ. D) Angular spreads as a function of Δ. Where two families of crystal planes appear at the same dihedral angle, they are distinguished by different symbols.

Asymmetric triradiate spicules from Sycon:[9b] The crystallographic orientation of these triradiate spicules can be regarded as a combination of the above-mentioned types, in the sense that two rays of each spicule develop perpendicular to the ($\bar{1}02$) and ($1\bar{1}2$) planes, and the third ray grows perpendicular to the ($0\bar{1}6$) calcite plane (Fig. 1F). So, although *Sycon* triradiates appear morphologically similar to the *Clathrina* symmetric triradiates, they are crystallographically quite different. The whole spicule also shows well-defined textural anisotropy within sets of symmetry-related crystallographic directions (Fig. 7A, B). Consistent with the observations made for the monaxon spicules, the

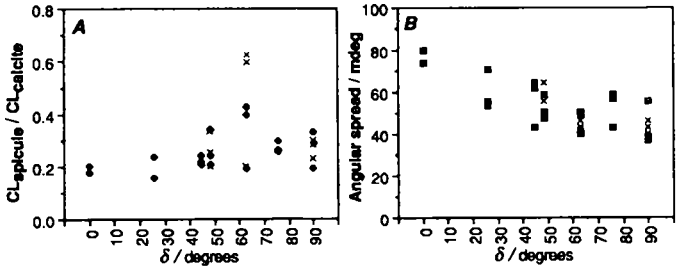

Fig. 7. Coherence lengths normalized to pure calcite (A) and angular spreads (B) for the diffraction peaks of one *Sycon* asymmetric triradiate spicule, plotted as a function of the dihedral angle δ. Where two families of crystal planes appear at the same dihedral angle, they are distinguished by different symbols.

larger coherence lengths and the smaller angular spreads are present in the crystallographic directions coincident with, or close to, the directions of the morphological axes of the spicule rays. However, the textural features obtained for the whole spicule correspond to the average values derived from the three differently oriented rays. In order to avoid this averaging effect, which may distort the real textural features, the anisotropy of every spicule ray was monitored separately for two triradiates. Figure 8 shows diffraction peak profiles of the representative {104} and {012} reflections for three rays of the same spicule.[10] In general, two symmetrical rays, which develop perpendicular

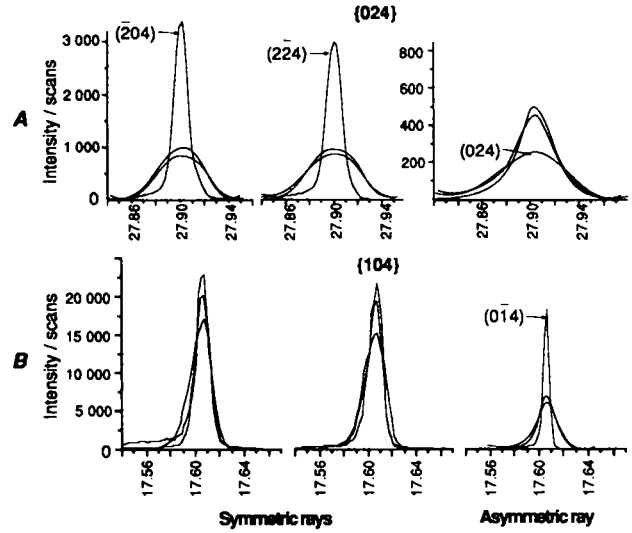

Fig. 8. Diffraction peak profiles of the {024} (A) and {104} (B) families of reflections for the three separated rays of one asymmetric triradiate spicule from *Sycon*. Note that the symmetric rays are elongated in the [$\bar{2}04$] and [$2\bar{2}4$] directions, and the asymmetric ray in the [$0\bar{1}6$] direction.

to the ($\bar{1}02$) and ($1\bar{1}2$) crystallographic planes, display textural features that are remarkably similar to those observed for the *Kebira* curved monaxons. The third ray, which grows roughly perpendicular to the ($0\bar{1}6$) crystallographic plane, is similar to the naillike *Kebira* spicule.

Discussion

In general, the morphological symmetry of a crystal is either higher or equal to the symmetry of its internal structure.[13] Under non-biogenic conditions, the internal structure dictates the morphological symmetry because crystal morphology is determined by the rate of growth of the crystal in the different directions.[14] The "rule of thumb" is that crystal planes perpendicular to directions of slow growth will develop into stable faces. The rate of addition of new layers in a given direction is in turn determined by the layer energy and by the interactions with the environment, including the solvent and cosolutes.[14] Symmetry-related planes have identical layer energies and identical surface interactions in an isotropic environment. Hence, in such an environment, the resulting morphology respects the symmetry of the component's structure. This restriction is certainly not applicable to crystals grown in biological environments, which may display morphological symmetries lower than the constituent structure and not related to it.

In this study we have examined three types of calcareous sponge spicules, which are all beautiful examples of how the biological environment induces a reduction in crystal symmetry. The *Kebira* giant monaxon has morphological symmetry *m*, the *Kebira* "nail" spicule *mm 2* (but not related to the calcite crystal axes), and the *Sycon* asymmetric triradiate spicule has symmetry *m*. They are each composed of one single crystal of calcite that has point group symmetry $\bar{3}m$. This peculiar reduction in morphological symmetry is achieved through the controlled introduction of macromolecules along specific crystallographic and morphological directions. The intercalation occurs during the formation of the crystals, where it modulates the crystal's growth in different directions. It does not change the crystal structure, but rather creates discontinuities in the perfect lattice. The presence of the macromolecules is permanently imprinted

0947-6539/95/0107-0418 $ 30.00+.25/0 Chem. Eur. J. 1995, 1, No. 7

as a modification in crystal microtexture (i.e., coherence length and angular spread). We have shown here that the anisotropy of the spicule morphology is closely matched by similar anisotropy in the textural parameters, irrespective of the crystallographic symmetry. For comparison, we have also examined the synthetic crystals, namely calcite and magnesium-containing calcite. In addition, the *Clathrina* triradiate spicule was included as an example of a calcareous sponge spicule whose morphology does reflect the symmetry of calcite. Figure 9 shows the three-dimensional plots of the vectors of all the coherence lengths for each crystal studied. These visually represent the symmetry of the perfect domains that constitute different crystals.

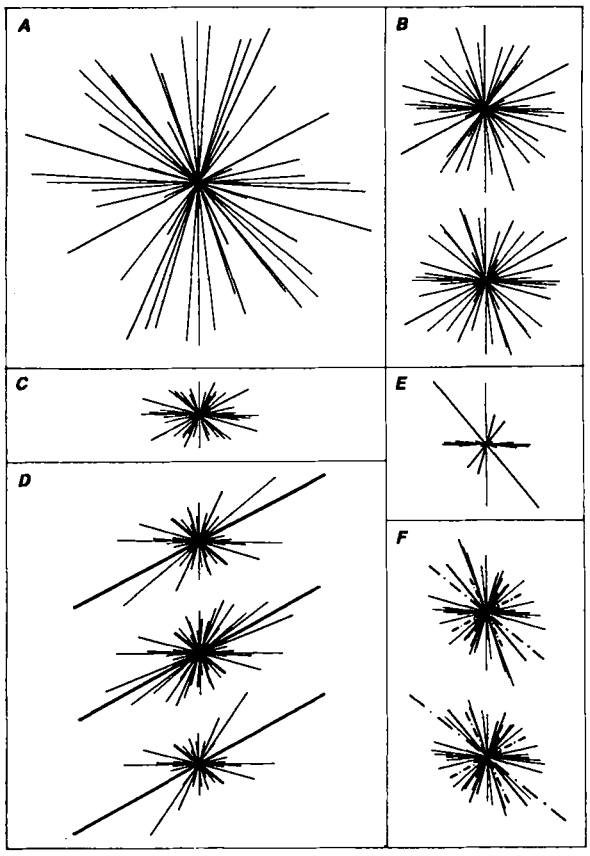

Fig. 9. Three-dimensional representation of the coherence lengths in all the measured crystals, drawn in the same orientation and to the same scale. Each line represents a vector originating at the center of the plot, whose length is proportional to the coherence length in a defined crystallographic direction, normalized to the corresponding value measured for the synthetic calcite crystal. The *c* axis is oriented vertically. A) Synthetic pure calcite. B) The two synthetic Mg-calcite crystals. C) *Clathrina* triradiate spicule. D) The three *Kebira* curved monaxons; the vectors of the symmetry-related {012} reflections are designated by thicker lines. E) *Kebira* "nail" spicule; the vectors of the symmetry-related {104} reflections are designated by thicker lines. F) The two *Sycon* asymmetric triradiate spicules measured intact. The vectors of the {104} and {012} families of reflections are represented by thicker and dashed lines, respectively.

Pure calcite is texturally isotropic, highly aligned, and preserves a coherent lattice organization up to micron-size domains (Fig. 9A). The experimental limitations, due to the intrinsic resolution of the instrument, combined with the empirical nature of the Scherrer formula, make it very difficult to establish an upper limit to the coherence length. The same limitations may obscure the detection of intrinsic lattice-dependent differences in coherence length in the different directions. In order to neutralize such effects, all the data on the biogenic crystals were normalized to pure calcite for each diffraction peak.

The synthetic calcite crystals containing magnesium ions are also isotropic in texture (Fig. 9B). Their angular spread, however, is increased by one order of magnitude relative to pure calcite, while the coherence length decreases by only a factor of two to three. In addition, the amount of magnesium in the crystals, as evaluated from atomic absorption, is larger than that deduced from the change in cell dimensions. These observations indicate that a significant portion of the magnesium ions are preferentially accumulated at existing dislocation sites, as opposed to being intercalated inside the lattice creating new dislocation sites. It cannot, however, be assumed that under biological conditions the same effects would occur. Organisms are able to introduce much more magnesium into their calcite crystals than can be achieved in vitro.[11b] The manner in which they do this, and consequently the effect on crystal texture, may thus also be different. We can only infer, on the basis of the data on synthetic crystals, that a small ion, introduced from an isotropic environment, has an isotropic effect on the crystal texture.

The *Clathrina* symmetric triradiate spicules that contain the largest percentage of magnesium are also isotropic in texture in the *ab* plane (Fig. 9C). This is consistent with their isotropic average morphology in this plane.[8] The other spicules display a distinctly anisotropic texture, which does not relate in any way to the crystal symmetry; this implies that organisms are able to differentially affect symmetry-related crystallographic directions, and thus overcome the intrinsic symmetry of the crystal (Fig. 9D–F). The observed reduction in symmetry within symmetry-related directions is highlighted for the families {012} and {104}.[10] These include the directions of major morphological development for the *Kebira* and *Sycon* spicules. The curved monaxons are examined in greater detail below, as an example of how much reduction in symmetry may be achieved.

The *Kebira* curved monaxons may be up to several millimeters in length. *Sycon* also produces curved monaxons with exactly the same morphology as *Kebira*, but much smaller. The volumes of the spicules from these two genera differ by up to two orders of magnitude. Surprisingly, the data from the two species are almost superimposable (spicules from *Sycon* have also been measured, and the results were reported separately[8]). In addition to providing credibility to the measurements, this identity shows that the properties measured are microscopically controlled and are not scale-dependent. This is particularly important for the angular spread, which could well be an additive and hence a volume-sensitive parameter.

By combining all the information available, the following picture of the curved monaxon spicule microtexture emerges: It consists of an assembly of perfectly coherent domains, each having roughly the shape of a cylinder. The long axis corresponds to [012] or close to it. Adjacent cylinders are misaligned relative to one another *around* the cylinders' axes. The misalignment *between* the cylinder axes is, however, almost negligible. The surface of the cylinder incorporates many different crystallographic directions, yet proteins are apparently intercalated at regular intervals along these directions, totally independently of the structure. This can be deduced from the observation that the textural properties perpendicular to the cylinder axis are almost isotropic. At this time we can only speculate on how this astounding level of control can be achieved in the biological environment, which ultimately results in the marked reduction in textural symmetry observed.

A crucial observation is that the positive direction of the calcite *c* axis is always oriented with the convexity of the spicule. This indicates that not only is there a distinction between three symmetry-related $\{hkl\}$ planes, but also between the positive and negative surfaces of the same plane ((hkl) relative to $(\bar{h}\bar{k}\bar{l})$).

  0947-6539/95/0107-0419 $ 30.00+.25/0

This additional type of reduction in symmetry can be achieved only through oriented nucleation. Although the location and structure of the actual nucleation plane is unknown, we deduce from the above that it cannot be of the type (001) or (*hk*0), because such planes are equivalent relative to the positive and negative directions of the *c* axis. The (012) plane is a good candidate and is useful for explaining how the positive and negative directions could be distinguished during nucleation. As [012] is the morphological axis of the spicule, nucleation would occur at the extremity of the spicule. The (012) plane is composed of layers of calcium ions, alternating with layers of carbonate ions (Fig. 10). The planar carbonate anions form an

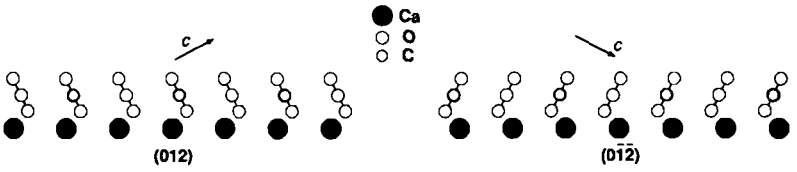

Fig. 10. Structure of the (012) crystallographic plane (left) compared to the (01$\bar{2}$) plane (right). The crystal growth direction is perpendicular to the layers of calcium and carbonate ions.

angle of 64° with the plane of calcium ions. The concept of oriented nucleation would imply in this case that the nucleating surface controls not only the assembly of the ions, but also determines the angle (64 or 116°) that the carbonate ions form with the nucleating surface. Interestingly, oriented nucleation of calcite crystals from the (012) plane with the same type of recognition has been observed on acidic polydiacetylene films.[15] We also note that biological discrimination between the positive and negative surfaces of the same crystal plane, achieved through the oriented nucleation of crystals, has also been described in magnetotactic bacteria[16] and coccoliths.[17]

After nucleation, crystal growth would proceed unidirectionally within a closed volume into which the cells secrete the ions and the macromolecules, which interact specifically with the crystal. These macromolecules would be selectively adsorbed on the matching surfaces that are exposed during growth, that is, on (001), (10$\bar{2}$), and ($\bar{1}$1$\bar{2}$) (and possibly other surfaces), but not on (01$\bar{2}$), which is blocked by the nucleating surface. As a result, crystal growth would be inhibited in all directions apart from [012], where spicule elongation is unimpeded. Thus, oriented nucleation, together with unidirectional growth in the presence of specific macromolecules, could result in the observed reduction in symmetry. This hypothesis is supported by morphological evidence showing that the intracrystalline macromolecules in vitro preferentially adsorb on faces of the type {01*l*} ($l \approx 2$) and {001}.[8]

An alternative explanation combines oriented nucleation with physically rather than chemically driven adsorption. Conceivably, macromolecule adsorption could be induced exclusively by physical contact between the membrane and the growing crystal at the site of secretion, or by gradients and directional flows inside the closed volume, which target the proteins to specific sites, regardless of the nature of the surfaces exposed. The presence of these driving forces should certainly not be underrated in biological environments. The combination of molecular recognition at the highest level on the nucleation site with its total absence during growth would be surprising, but is not inconceivable.

Analogous arguments can be invoked for the other two spicule types—the "nail" spicule from *Kebira* (Fig. 9E) and the asymmetric triradiate spicules from *Sycon* (Fig. 9F). The latter has two equivalent rays developing in the [$\bar{1}$02] and [1$\bar{1}$2] directions, and one in the [0$\bar{1}$6] direction. Each one of these rays must be considered as an element on its own, as far as growth control is concerned. The overall textural picture would be expected to be a combination of the three, and thus somehow distorted. Indeed, textural measurements of the separated rays of the asymmetric spicule unequivocally show the extent of reduction in symmetry that can be achieved for each of the growing subunits of the same crystal (Fig. 11). The average shapes of the highly anisotropic perfect domains of each spicule ray reflect the macroscopic morphology to a remarkable degree.

To the best of our knowledge, this is the first demonstration of reduction in crystal symmetry at the textural level, without a concomitant reduction in the intrinsic symmetry of the crystal structure. It is conceivable that such textural effects also occur in solid solutions formed by "tailor-made" inhibitors within crystals.[18] These, however, have not been monitored. This higher level of control is reminiscent of the effect of chirally resolved amino acids on crystals of chiral racemic (serine) or achiral (glycine) α-amino acids, where reduction in symmetry occurs concomitantly with the choice of specific sectors and with reduction in morphological symmetry of the crystal.[5] It is even more striking in the biogenic crystals, because the carbonate molecule does not display obviously chiral or prochiral centers. In relation to chirality, it is noteworthy that etch pits of enantiomorphous shapes were induced by tartaric, malic, and lactic acid on calcite crystals.[19] Whether the chiral nature of the protein is directly involved in the mechanism of growth of the biogenic crystals is impossible to establish at this stage. This is but one additional facet of interest in the understanding of the complex process of crystal growth by organisms, which is a most intriguing manifestation of molecular control exerted in nature.

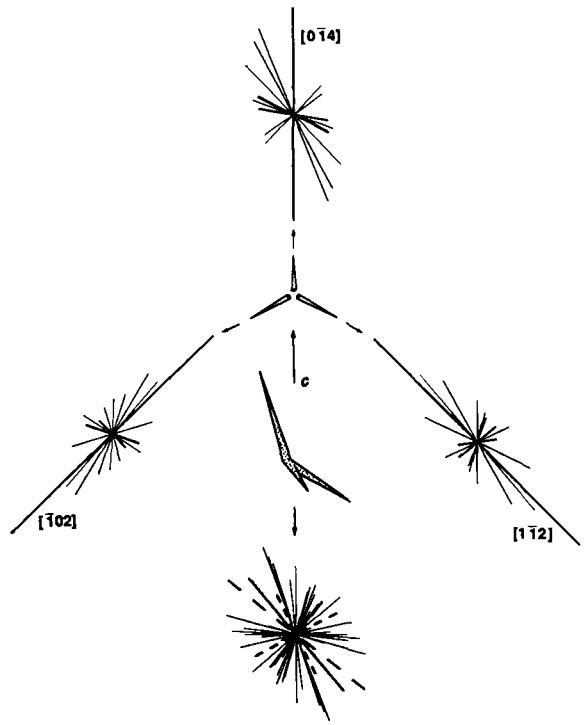

Fig. 11. Textural anisotropy of the separated rays of the same asymmetric triradiate spicule (top) relative to the intact spicule (bottom). The coherence length vectors are defined as in Fig. 9.

0947-6539/95/0107-0420 $ 30.00+.25/0

Materials and Methods

Materials: Calcareous sponges *Clathrina contorta*, *Sycon* sp. (eastern Mediterranean), and *Kebira uteoides* (Red Sea) were collected, washed with fresh water, and rapidly frozen in liquid nitrogen, in order to avoid dissolution of the spicules or crystallization of calcium carbonate on the spicules. After thawing, the tissues were treated with 2.5% sodium hypochlorite solution and placed on a rocking table for 1 h. The spicule suspension was then rapidly rinsed several times with doubly distilled water, and the cleaned spicules were air-dried. Specimens of symmetric triradiate spicules from *Clathrina*, "nail" spicules and curved monaxon spicules from *Kebira*, and asymmetric triradiate spicules from *Sycon* were selected for further study. In order to separate the individual rays of the same asymmetric triradiate spicule without introducing stress in the crystal, a small drop of dilute HCl solution (pH = 5) was placed at the point of intersection of the rays. The separated individual rays were immediately rinsed with doubly distilled water and air-dried.

Synthetic calcite crystals were grown by slow diffusion of ammonium carbonate vapor into a 7.5 mM calcium chloride solution or into a mixture of 25 mM calcium chloride and 5 mM magnesium chloride solutions. Magnesium contents were determined from the reduction in the calcite cell dimensions by using X-ray diffraction [11].

Synchrotron X-Ray Diffraction Measurements: Selected individual spicules and synthetic crystals were glued to thin glass fibers in different orientations to eliminate a possible effect of their position relative to the beam on crystal texture. The fibers were attached to brass pins. Determination of the orientation matrix and preliminary measurements were performed on a Rigaku rotating Cu-anode four-circle diffractometer, equipped with a Siroflux double monochromator condensing–collimating system. As calcite crystals are extremely ordered, their fine textural parameters are beyond the resolution of standard X-ray equipment. High-resolution diffraction peak profiles were therefore collected by using well-collimated synchrotron X-radiation at the National Synchrotron Light Source at Brookhaven National Laboratory (line X7B). The line is equipped with a six-circle Huber diffractometer, with reducing gears on ω, 2θ, χ, and ϕ, and on the analyzer ω and 2θ, to allow a maximum step-to-step resolution (sampling frequency) of 5×10^{-4} deg on θ and ω [7]. A Ge(220) analyzer crystal was mounted on the detector arm; this made it possible to deconvolute the ω and $\omega/2\theta$ profiles. In the ω-scan mode, the detector is fixed at the Bragg angle 2θ, and the crystal is rotated about the diffractometer main axis by an angle $\Delta\omega$. The peak width in this mode provides information on the angular dispersion of the mosaic blocks within the crystal. In the $\omega/2\theta$ scan mode, the rotation of the detector by $2\Delta\theta$ follows the rotation of the crystal by $\Delta\omega$, where $\Delta\omega = \Delta\theta$. Thus, the peak broadening due to angular spread is excluded, and the size of perfect domains can be determined. Every profile consisted of 100 data points with sampling frequencies of 0.004° for the ω scans and 0.001/0.002° for $\omega/2\theta$ scans, respectively. For the highly ordered synthetic calcite crystal, sampling frequencies in the two modes were 0.0005° (ω) and 0.0005/0.001° ($\omega/2\theta$). The measurement parameters and the characteristics of the $\omega/2\theta$ scans of the same reflections for all crystals examined are shown in Table 1.

Table 1. Measurement parameters and the characteristics of the $\omega/2\theta$ scans for all crystals examined.

Crystal type	Number of reflections collected	Magnesium content (mol.%)	$\omega/2\theta$-scan parameters {1 0 4} Bragg angle	Max. intensity	Integrated intensity	Signal/noise ratio[a]	FWHM[b] (mdeg)	{0 1 2} Bragg angle	Max. intensity	Integrated intensity	Signal/noise ratio[a]	FWHM[b] (mdeg)
Pure calcite	28	-	8.722	5 700	27 930	800	4.9	6.860	1 120	6 890	550	6.2
			8.722	5 140	28 110	650	5.5	6.860	910	5 300	450	5.8
Mg-calcite 1	24	2.5	8.724	21 090	144 000	300	13.7	6.860	2 370	15 110	150	12.8
			8.723	22 080	141 950	250	12.9	6.861	3 450	17 490	200	10.2
			8.725	24 370	169 040	200	13.9	6.861	2 140	14 980	120	14.1
Mg-calcite 2	23	3.0	8.724	7 040	72 020	120	20.6	13.821[c]	700	7 790	20	23.4
			8.724	5 820	58 900	70	20.5	13.817	485	7 630	30	32.7
			8.726	6 920	63 920	80	18.7	13.820	870	12 100	35	28.6
Clathrina spicule	26	16.0	8.840	835	12 030	170	29.0	6.936	395	2 670	10	15.2
			8.846	855	12 000	70	28.6	6.937	340	3 080	9	20.5
			8.844	710	10 700	50	30.8	6.933	535	3 500	13	14.1
Kebira monaxon 1	25	18.0	8.866	6 020	86 790	110	29.1	6.960	7 100	25 050	> 1 000	7.1
			8.862	7 470	85 640	25	23.9	6.958	1 390	17 620	100	25.6
			8.863	7 590	91 120	40	24.1	6.961	1 490	17 520	200	23.6
Kebira monaxon 2	38	17.0	8.843	11 300	140 090	100	25.1	6.938	4 810	15 820	> 1 000	6.6
			8.843	9 800	110 730	180	22.7	6.938	950	11 210	110	23.8
			8.84	9 450	107 750	75	23.1	6.937	800	10 330	200	26.0
Kebira monaxon 3	25	16.5	8.851	3 670	53 140	130	29.1	6.951	20 850	65 120	300	6.3
			8.856	4 100	52 600	190	25.8	6.949	5 320	70 990	120	26.9
			8.856	5 820	71 000	65	24.8	6.950	3 010	38 430	80	25.9
Kebira "nail" spicule	10	14.0	8.840	3 290	15 980	50	9.9					
			8.838	1 600	14 240	12	20.7					
			8.839	2 190	20 970	35	19.7					
Sycon triradiate 1	29	13.5	8.820	39 780	307 900	70	15.7	6.929	790	11 820	20	31.2
			8.823	24 030	296 600	180	24.8	6.929	1 740	12 330	400	14.2
			8.819	29 420	330 920	150	22.7	6.932	1 600	12 190	450	15.3
Sycon triradiate 2	25	13.0	8.804	69 900	509 500	700	14.6	6.913	13 070	171 470	300	26.3
			8.804	43 080	443 010	300	20.6	6.914	31 740	140 190	> 1 000	8.8
			8.804	45 100	442 710	300	19.7	6.914	29 640	136 680	400	9.2
Sycon triradiate 31	16	13.5	8.820	7 230	94 160	90	24.1	13.963[c]	6 380	39 350	800	12.1
			8.820	9 780	89 870	170	17.3	13.960	2 090	42 590	140	39.6
			8.819	10 010	101 650	150	19.1	13.962	1 700	38 600	170	44.5
Sycon triradiate 32	25	13.0	8.816	4 450	60 890	110	25.8	6.922	2 660	10 040	> 1 000	7.4
			8.815	5 660	63 720	50	18.9	6.925	720	10 210	180	27.4
			8.816	6 220	62 340	70	17.4	6.923	810	10 470	270	25.2
Sycon triradiate 33	13	13.0	8.811	3 400	15 110	240	8.1	6.919	100	2 240	14	33.1
			8.812	2 000	19 820	40	15.2	6.920	130	1 890	18	19.0
			8.812	1250	14 570	60	20.3	6.918	150	2 060	20	18.4
Sycon triradiate 41	14	13.0	8.805	17 100	183 400	710	21.2	13.957[c]	3 370	24 950	> 1 000	14.7
			8.804	20 200	168 340	900	16.5	13.956	920	21 540	70	44.6
			8.804	23 150	189 820	320	15.8	13.955	1 070	25 860	60	45.8
Sycon triradiate 42	16	13.0	8.803	15 250	174 250	> 1 000	22.7	13.955[c]	3020	24 000	480	15.5
			8.805	21 700	195 430	180	17.0	13.955	1 020	27 540	60	51.5
			8.804	19 450	161 460	600	16.3	13.956	920	25 230	90	53.1
Sycon triradiate 43	13	12.5	8.801	16 750	72 900	600	8.4	13.950[c]	260	9 020	50	66.7
			8.800	7 250	74 750	120	19.1	13.951	520	10 600	60	38.1
			8.801	6 900	74 350	110	20.1	13.951	460	10 950	20	39.6

[a] Maximum intensity divided by the mean background value. [b] Full width at half maximum. [c] The {024} family of reflections is presented instead of the {012}.

Data Analysis: Two parameters of crystal texture were derived from analysis of the peak profiles. The coherence length (CL) was calculated applying the Scherrer formula [12] [Eq. (1)] to the diffraction peak width measured in the $\omega/2\theta$ scan

$$CL = \frac{\lambda}{\cos\theta\sqrt{B^2_{\omega/2} - \beta^2}} \quad (1)$$

mode, where λ is the wavelength, θ the Bragg angle, and β the instrumental resolution expressed in radians. In our setup, $\lambda = 0.9195$ Å and $\beta = 0.003°$. The peak width, $B_{\omega/2}$ (in radians), was determined from the integrated intensity of the peak divided by its maximum intensity after subtracting the background level. When $B^2_{\omega/2} < 2\beta^2$, i.e., $B < 4.3 \times 10^{-3}°$, subtraction of the instrumental resolution results in unreliably high values of coherence length. These peaks were discarded from the calculation of coherence length. In the ω scan mode, the peak width at half height is taken to correspond to the average angular spread of the domains directly.

The Scherrer formula includes a multiplicative constant K that is shape-dependent and may assume values $0.5 < K < 2.0$ [20]. In the present data analysis, K is taken to be equal 1, although the crystal morphologies are not spherically symmetric. We note, however, that while it is difficult to exactly evaluate K for these complicated morphologies, the application of appropriate values of $K \neq 1$ would, in all cases, further exaggerate the observed anisotropies. For example, for thin plates the values of K for directions in the plane of the plate are greater than 1, as is the K value in the direction of elongation for needle-shaped crystals. This means that the coherence lengths in morphologically more developed directions are even larger than those calculated with $K = 1$.

Acknowledgments: We thank Dr. Micha Ilan, Tel Aviv University, for help in collecting the specimens and advising us about sponge biology. We also thank Dr. Felix Frolow for his help in setting up the Siroflux system. S. W. is the incumbent of the I. W. Abel Professorial Chair of Structural Biology, and L. A. of the Patrick E. Gorman Professorial Chair of Biological Ultrastructure. This study was funded in part by the Kimmelman Center for Biomolecular Structure and Assembly, and by grant No. 92-00100 from the US–Israel Binational Science Foundation. The research was carried out at Brookhaven National Laboratory under contract DE-AC02-76CH00016 with the US Department of Energy and supported by its Division of Chemical Sciences, Office of Basic Energy Sciences.

Received: January 18, 1995 [F59]

  0947-6539/95/0107-0421 $ 30.00+.25/0

[1] a) K. Simkiss, K. M. Wilbur, *Biomineralization. Cell Biology and Mineral Deposition*, Acad. Press, San Diego, **1989**; b) H. A. Lowenstam, S. Weiner, *On Biomineralization*, Oxford Univ. Press, New York, **1989**; c) S. Mann in *Biomineralization. Chemical and Biochemical Perspectives* (Eds.: S. Mann, J. Webb, R. J. P. Williams), VCH, Weinheim, **1989**, pp. 189–222; d) S. A. Wainwright, W. D. Biggs, J. D. Currey, J. M. Gosline, *Mechanical Design in Organisms*, John Wiley, New York, **1976**.

[2] a) A. Berman, L. Addadi, S. Weiner, *Nature* **1988**, *331*, 546–548; b) L. Addadi, S. Weiner, *Angew. Chem. Int. Ed. Engl.* **1992**, *81*, 153–166.

[3] a) J. M. McBride, S. B. Bertman, *Angew. Chem. Int. Ed. Engl.* **1989**, *28*, 330–333; b) I. Weissbuch, L. Addadi, M. Lahav, L. Leiserowitz, *Science* **1991**, *253*, 637–645; c) Y. Weisinger-Lewin, F. Frolow, R. K. McMullan, T. F. Koetzle, M. Lahav, L. Leiserowitz, *J. Am. Chem. Soc.* **1989**, *111*, 1035–1040; d) A. M. Cody, R. D. Cody, *J. Crystal Growth* **1991**, 508–519; e) B. Kahr, J. M. McBride, *Angew. Chem. Int. Ed. Engl.* **1992**, *31*, 1–26.

[4] a) R. J. Reeder, *Nature* **1991**, *353*, 797–798; b) W. J. Staudt, R. J. Reeder, M. A. A. Schoonen, *Geochim. Cosmochim. Acta* **1994**, *58*, 2087–2098; c) H. E. Buckley, *Crystal growth*, John Wiley, New York, **1958**, pp. 339–387; d) M. P. Kelley, B. Janssens, B. Kahr, *J. Am. Chem. Soc.* **1994**, *116*, 5519–5520.

[5] a) L. Addadi, Z. Berkovitch-Yellin, I. Weissbuch, M. Lahav, L. Leiserowitz, S. Weinstein, *J. Am. Chem. Soc.* **1982**, *104*, 2075–2077; b) I. Weissbuch, L. Addadi, Z. Berkovitch-Yellin, E. Gati, S. Weinstein, M. Lahav, L. Leiserowitz, *J. Am. Chem. Soc.* **1983**, *105*, 6613–6620.

[6] S. Albeck, J. Aizenberg, L. Addadi, S. Weiner, *J. Am. Chem. Soc.* **1993**, *115*, 11691–11697.

[7] a) A. Berman, J. Hanson, L. Leiserowitz, T. F. Koetzle, S. Weiner, L. Addadi, *Science* **1993**, *259*, 776–779; b) A. Berman, J. Hanson, L. Leiserowitz, T. F. Koetzle, S. Weiner, L. Addadi, *J. Phys. Chem.* **1993**, *97*, 5162–5170.

[8] J. Aizenberg, J. Hanson, M. Ilan, L. Leiserowitz, T. F. Koetzle, L. Addadi, S. Weiner, *FASEB J.* **1995**, *9*, 262–268.

[9] a) E. A. Minchin, *Quart. J. Micr. Sci.* **1898**, *40*, 469–587; b) W. C. Jones, *Quart. J. Micr. Sci.* **1955**, *96*, 129–149; c) W. C. Jones, D. W. F. James, *Micron* **1972**, *3*, 196–210; d) M. Ilan, J. Vacelet, *Ophelia* **1993**, *38*, 107–116.

[10] In hexagonal space groups, the symmetry-related $\{hkl\}$ reflections are (hkl), $(k,-(h+k),l)$, $(-(h+k),h,l)$, and their Friedel pairs. For example, for the $\{012\}$ family, the symmetry-related reflections are (012), $(\bar{1}02)$, $(1\bar{1}2)$, $(0\bar{1}\bar{2})$, $(10\bar{2})$, and $(\bar{1}1\bar{2})$. For $\{104\}$, they are (104), $(0\bar{1}4)$, $(\bar{1}14)$, and their Friedel pairs.

[11] J. R. Goldsmith, D. L. Graf, H. C. Heard, *Am. Mineral.* **1961**, *46*, 453–457.

[12] a) A. Guinier, *X-Ray Diffraction in Crystals, Imperfect Crystals, and Amorphous Bodies*, W. H. Freeman, San-Francisco, **1963**; b) H. P. Klug, L. E. Alexander, *X-Ray Diffraction Procedures*, 2nd ed., Wiley-Interscience, New York, **1974**.

[13] P. Curie, *J. Phys. (Paris)*, **1894**, p. 393.

[14] a) P. Hartman, W. G. Perdok, *Acta Cryst.* **1955**, *8*, 49–52; *ibid.* **1955**, *8*, 521–529; b) Z. Berkovitch-Yellin, *J. Am. Chem. Soc.* **1985**, *107*, 8239–8249.

[15] A. Berman, D. J. Ahn, A. Lio, M. Salmeron, A. Reichert, D. Charych, *Science* **1995**, *269*, 515–518.

[16] a) S. Mann, N. H. C. Sparks, R. P. Blakemore, *Proc. R. Soc. Lond.* **1987**, *B231*, 477–487; b) S. Mann, N. H. C. Sparks, R. G. Board, *Advances in Microbial Physiology* **1990**, *31*, 125–181.

[17] a) S. Mann, N. H. C. Sparks, *Proc. R. Soc. Lond.* **1988**, *B234*, 441–453; b) J. R. Young, J. M. Didymus, P. R. Bown, B. Prins, S. Mann, *Nature* **1992**, *356*, 516–518; c) J. M. Didymus, J. R. Young, S. Mann, *Proc. R. Soc. Lond.* **1994**, *B258*, 237–245.

[18] J. L. Wang, Z. Berkovitch-Yellin, L. Leiserowitz, *Acta Cryst.* **1985**, *B41*, 341–348.

[19] a) A. P. Honess, *The Nature, Origin and Interpretation of the Etch Figures on Crystals*, John Wiley, New York, **1927**; b) H. E. Buckley, *Crystal growth*, John Wiley, New York, **1958**, pp. 304–338; c) J. M. Thomas, G. D. Renshaw, C. Roscoe, *Nature* **1964**, *203*, 72–73.

[20] a) B. E. Warren, *Phys. Rev.* **1941**, *59*, 693–699; b) A. R. Stokes, A. J. C. Wilson, *Proc. Camb. Phil. Soc.* **1942**, *38*, 313–322; c) B. E. Warren, P. Bodenstein, *Acta Cryst.* **1965**, *18*, 282–286; **1966**, *20*, 602–605; d) R. Perret, W. Ruland, *J. Appl. Cryst.* **1968**, *1*, 257–262.

0947-6539/95/0107-0422 $ 30.00+.25/0